Imaging molecules from within: Ultrafast angström-scale structure determination of molecules via photoelectron holography using free-electron lasers

F. Krasniqi,[1] B. Najjari,[2] L. Strüder,[1,3] D. Rolles,[1] A. Voitkiv,[2] and J. Ullrich[1,2]
[1]*Max Planck Advanced Study Group, Center for Free Electron Laser Science, Hamburg, Germany*
[2]*Max-Planck-Institut für Kernphysik, Saupfercheckweg 1, D-69117 Heidelberg, Germany*
[3]*MPI Halbleiterlabor, Otto-Hahn-Ring 6, D-81739 München, Germany*
(Received 16 October 2009; published 18 March 2010)

A scheme based on (i) upcoming brilliant x-ray free-electron laser (FEL) sources, (ii) innovative energy and angular-dispersive large-area electron imagers, and (iii) the well-known photoelectron holography is elaborated that provides time-dependent three-dimensional structure determination of small to medium-sized molecules with Ångström spatial and femtosecond time resolution. Inducing molecular dynamics, wave-packet motion, dissociation, passage through conical intersections, or isomerization by a pump pulse this motion is visualized by the x-ray FEL probe pulse launching keV photoelectrons within a few femtoseconds from specific and well-defined sites, deep core levels of individual atoms, inside the molecule. On their way out, the photoelectrons are diffracted generating a hologram on the detector that encodes the molecular structure at the instant of photoionization, thus providing "femtosecond snapshot images of the molecule from within." Detailed calculations in various approximations of increasing sophistication are presented and three-dimensional retrieval of the spatial structure of the molecule with Ångström spatial resolution is demonstrated. Due to the large photoabsorption cross sections the method extends x-ray-diffraction-based time-dependent structure investigations envisioned at FEL's to new classes of samples that are not accessible by any other method. Among them are dilute samples in the gas phase such as aligned, oriented, or conformer-selected molecules, ultracold ensembles and/or molecular or cluster objects containing mainly light atoms that do not scatter x rays efficiently.

DOI: 10.1103/PhysRevA.81.033411 PACS number(s): 33.80.Eh, 33.60.+q, 87.64.Bx

I. INTRODUCTION

The vision to directly follow time-dependent structural changes when molecular bonds are formed or break apart, when transition states or conical intersections are passed, namely to "make the molecular movie" on atomic (i.e., subnanometer length) and molecular (i.e., femtosecond) time scales is among the strongest motivations driving huge efforts worldwide to develop next-generation light sources, the free-electron lasers (FEL) [1–5]. Delivering ultra-intense bursts of 10^{13} coherent photons at up to 12 keV energies with pulse lengths of 10 to 100 fs and realistic prospects to reach 1 fs in the future, the "standard" scenario is to extract the (time-dependent) structure of molecules in the gas phase via coherent x-ray diffraction. Focusing the x rays to spots as small as 100 nm onto single objects, this extends the hope of imaging individual molecules in the gas phase [6]. This will, in principle, enable (time-dependent) structure determinations of many noncrystalizable molecules of biological interest, considered to represent a major breakthrough in structural biology.

Nevertheless, the realization of these visions is by far not assured essentially due to two reasons. First, even though the photon flux is huge, the tiny x-ray diffraction cross section of typically $\sim 10^{-24}$ cm^2 results in just a few tens to a few thousands of scattered photons in one shot from, for example, an aligned gas phase molecular ensemble or from a large single molecule, respectively. Thus, thousands of individual shots with known relative orientation of the molecules have to be summed to obtain the statistical significance requested for atomic spatial resolution. Up to now there is no pathway identified without controversy to reach that goal. Second, the "destructive" photoabsorption cross section is factors of ten (e.g., for the carbon K shell in biomolecules) to a thousand (for heavier elements) larger compared to the one for coherent diffraction of 12 keV photons causing ultrafast delocalization of core level (via the direct photo effect) and outer-shell electrons (via the Auger effect with typical time constants of below 10 fs) culminating in the question whether the molecular structure will be first imaged and then destroyed or vice versa. Presently, common knowledge is that the maximum tolerable pulse length will be 10 fs and many investigations concentrate on the destruction issue placing scarifying layers around the object of interest [7,8].

As an alternative "table-top" method, femtosecond electron diffraction (FED) was suggested and developed to reach the previous goals on various fronts using "conventional guns" [9,10], envisioning intense laser-accelerated electron bunches [11], or using "rescattered" electrons in above-threshold ionization [12]. Due to an elastic scattering cross section that is larger by about a factor of $\sim 10^6$ for 30 keV electrons compared to 12 keV photons, along with the fact that inelastic destructive reactions (electron impact excitation) occur with smaller cross sections and a factor of a thousand less energy deposition compared to photon absorption, the number of electrons in the beam needed to record images as well as unwanted modifications of the sample molecules are significantly reduced [10]. In the most promising "conventional gun" scenario, bunches of up to 10^5 electrons of 30 keV within $\sim$600 fs focused to spot sizes of 200 μm were recently demonstrated to be feasible and structural information was achieved. 100 fs pulse durations for bunches of 10^4 electrons seem to be feasible optimizing existing gun designs [10].

Both methods, x-ray and electron diffraction, were extensively discussed and compared in the literature [10,13].

 ©2010 The American Physical Society

The drawbacks on the electron side are that it will be very challenging, if not impossible, to reach 100 fs time scales and below, the relatively large beam divergence and thus lower spatial resolution, missing coherence, and, most challenging, the so-called phase match problem when extended samples (200 μm) have to be used (like molecular ensembles in the gas phase): Due to the difference in velocity between the pump photons, initiating the dynamics, and the probe electron pulse of about a factor of 4 (30 keV electrons), the latter needing around picoseconds for traversing the sample region, a phase mismatch between pump and probe occurs not to be overcome by shortening the pulses, essentially absent in all optical setups.

In this article we present a third scheme along with model calculations, combining the best of the previously described worlds enabling us to realize the molecular movie with femtosecond time and Ångström spatial resolution for small and medium-sized molecules. It relies on the availability of x-ray FEL's as well as of novel high-speed readout, energy dispersive electron imaging devices (pnCCD see Ref. [14]) and is based on the well-known photoelectron holography scenario (see Refs. [15–17] and references therein). Along those lines and as schematically depicted in Fig. 1, it is suggested to utilize the x-ray FEL pulse to produce high-energy (500 eV to 2 keV), femtosecond-pulsed and monochromatic photoelectrons in individual molecules in a gas-phase sample by exploiting the otherwise "destructive" photoabsorption effect with its large cross section. As illustrated in Fig. 1, a linearly polarized x-ray FEL photon of energy $\hbar\omega$ is absorbed by a specific atom within the molecule, serving as an emitter of a photoelectron wave, which is embedded in a gas-phase ensemble of small

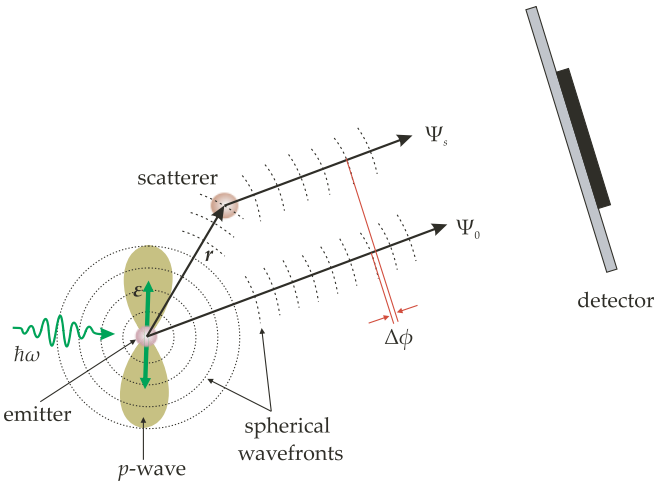

FIG. 1. (Color online) The principle of photoelectron holography (as outlined in Ref. [18]). A photoelectron p wave is emitted from one of the atoms in the molecule via absorption of linear polarized light with photon energy $\hbar\omega_\gamma$ from the K shell of the emitter with emerging spherical wavefronts. In photoelectron holography a photoelectron diffraction pattern is viewed as an interference between that part of the photoemitted wave, which propagates undisturbed into the detector Ψ_0, becoming a reference wave, and the part scattered by the nearby atoms Ψ_s, becoming an object wave which carries the information about the atomic positions. Ψ_0 and Ψ_s interfere on the detector with a phase shift $\Delta\phi$ yielding thus an intensity distribution $I_{\mathbf{p}} = |\Psi_0 + \Psi_s|^2$, which represents a hologram in a large portion of **p** space.

to medium-sized (some ten atoms) oriented molecules with mainly light constituent atoms ($Z < 20$). On "the way out," one part of the photoelectron wave (the object wave) is elastically scattered by the surrounding atoms (scatterers) whereas the other one (the reference wave) propagates undisturbed into the detector and interference between them leads to variations in the measured photo emission intensity, which encode the structural information as the holographic fringes revealing, among others, the three-dimensional (3D) relative Cartesian coordinates (i.e., the spatial structure of the molecule). This method contains the prerequisites of holography in a Gabor's sense [19], a reference wave and an object wave, and since the binding energies of the emitter atom are characteristic to its elemental identity and separated by the core levels of the scatterers, it is distinguished from the aspects of classical-slit diffraction as suggested by Cohen and Fano [20] and recently reviewed in Ref. [21]. A hologram recorded in a large portion of p space by a high-energy (>500 eV) electron imager (e.g., a pnCCD) can be analyzed in terms of phased Fourier transformation (see Ref. [22]) to yield real space images that locate individual atoms surrounding the emitter. This technique thus represents a different approach compared to previous concepts combing synchrotron radiation, low-energy photoelectron diffraction, and reaction microscopes that allow one for coincident detection of the 3D vector momenta of molecular fragments and photoelectrons from free, simple diatomic molecules "fixed-in-space" within the limits of the axial-recoil approximation (see Ref. [23] and our discussion in the following regarding basic concepts and comparison with other techniques).

The method exploits the fact that photoabsorption cross sections are of the order of $\sigma_{\text{photo}} \sim 10^{-20}$ cm^2 at about 1 keV above an edge and thus typically four orders of magnitude larger than those for coherent photon scattering with $\sim 10^{-24}$ cm^2 for 10 keV photons and carbon atoms. With a target line density of $\sim 10^{11}$ molecules/cm^2 and a photon flux of 10^{13} photons/pulse one can produce up to 10^4 electrons/pulse. Since each individual electron is created "on the spot" with atomic spatial precision (i.e., at individual molecules) it represents a huge effective current density in the order of 10^{10} A/cm^2 per electron on an area of (10 Å)^2 for an electron velocity of several 10^9 cm/s corresponding to keV energies and thus the total effective current density of 10^4 electrons in the pulse reaches $\sim 10^{14}$ A/cm^2 per pulse and $\sim 10^{16}$ A/cm^2 per second for an FEL repetition rate of 120 Hz. This compares with the optimistic $\sim 10^8$ A/cm^2 per second that might be achieved in FED experiments assuming $\sim 10^4$ electrons/pulse focused to a spot diameter of 200 μm with a pulse length of 100 fs, an electron energy of 30 keV, and a gun repetition rate of 1 MHz.

Therefore, if combined with a large solid-angle, high-efficiency multihit, energy-dispersive detectors, the method allows one to explore a whole class of molecules that can only be prepared as dilute samples with densities between 10^6 to 10^{11} cm^{-3} as typical for aligned [24], oriented [25], or even conformer-selected ensembles [18,26], all not accessible for pump-probe structure determination by any other present techniques. Here we built on the tremendous recent development in adiabatic [24] or pulsed laser alignment (for a recent review see Ref. [27]) as well as in Stark acceleration

[28] techniques to manipulate and define the molecular state where an unprecedented degree of laser-induced alignment and orientation was demonstrated [25].

The present article is aimed at providing the basic ideas and numbers for femtosecond photoelectron diffraction (FPED), illustrated using the chlorine-benzene molecule and verified by simple model calculations based on the well-known concepts of photoelectron holography. We also point to the limitations of the method and develop realistic scenarios for the 3D momentum imaging of the photoelectrons by exploiting forefront pnCCD x-ray pixel cameras.

II. BASIC CONCEPT AND COMPARISON WITH OTHER METHODS

In the scenario illustrated in Fig. 1, we produce the photoelectron inside of an individual molecule in the sample with femtosecond time and $\sim 10^{-3}$–10^{-4} relative energy resolution, ultimately limited by the FEL radiation properties (here, seeded beams are envisioned for the future with 1 fs or even sub-fs time resolution). On its way out the photoelectron wave, launched at one specific atom of the molecule (emitter) is partly diffracted on the individual atoms of the parent molecule (scatterers), as depicted in Fig. 1 for the most simple situation of only one scatterer, or reaches the detector directly, representing a reference wave for the scattered part. As described in Ref. [16] the electron wave with wavelength λ is fully coherent over a length of $l_c = \lambda^2/\Delta\lambda$ (i.e., over distances of $\sim$10 to $\sim$0.1 nm in the worst case) safely across medium-sized molecules, for an energy uncertainty of the FEL beam of $\Delta E_\gamma/E_\gamma \sim 10^{-4}$ at a few keV, translating in an uncertainly of the photoelectron energy of $\Delta E_e/E_e \sim 10^{-3}$-$10^{-4}$. Thus, a hologram is generated at the detector and, if the diffraction pattern is recorded over a large part of the solid angle, it allows one an immediate interpretation for photoelectron energies beyond $\sim$500 eV.

At the same time we transfer the nm wavelength of 1 to 10 keV photons to an electron deBroglie wavelength $\lambda_e = h/\sqrt{2m_e E_e}$ between $\sim$0.6 to 0.3 Å for $E_e = 500$ eV or $E_e = 2$ keV photoelectrons, respectively, allowing us to achieve Ångström spatial resolution as demonstrated recently [17].

To retrieve the structure of the molecule from the hologram on the detector, 3D electron momentum $\mathbf{P}_e = (p_x, p_y, p_z)$ images have to be recorded covering a large part of the final momentum space. This is achieved with an energy dispersive pixel pnCCD detector, as described later, determining two momentum components from the electron hitting position on the detector and the third one from the measured energy of the photoelectron $E_e = \hbar\omega_\gamma - I_{n,l}$ via energy-momentum conservation relations ($\hbar\omega_\gamma$ is the photon energy and $I_{n,l}$ is the binding energy of the atomic n, l shell that is photoionized). Electrons are emitted from molecules that are aligned, oriented, or conformer selected by methods [18,24–28] described in some detail later.

The method as proposed here comprises several concepts, builds on forefront technologies in various areas, and combines them in a unique way:

(i) Exploiting the new FEL light sources delivering intense (10^{13} photons per pulse), short-time ($\sim$100 fs with prospects of achieving 1 fs or even below), and coherent vacuum ultraviolet (vuv) or x-ray pulses with energies of 100 eV $< \hbar\omega_\gamma <$ 12 keV [1–5].

(ii) Building on the ability to align, orient, or conformer select in 3D space the molecules of interest with major progress achieved in the recent past [18,24–28].

(iii) Using high-energy electrons (500 eV $< E_e <$ 2 keV) for diffraction where the patterns are much simpler for interpretation in terms of photoelectron holography [15–17,29,30].

(iv) Applying a concept for 3D electron momentum imaging based on recently developed, large area, energy and position dispersive, single-electron counting pnCCD detector devices [14].

(v) Creating the photoelectrons directly by the x-ray pulse we do have an effective "all optical approach" in pump-probe experiments, thus, not facing the phase matching problem as in FED measurements using conventional electron guns [10].

Thus, our method represents a major step forward compared to all previous concepts as so-called molecular frame photoelectron angular distribution (MFPAD) spectroscopy being now a standard technology at synchrotron radiation facilities. Based on a recent experimental breakthrough in angle-resolved photoelectron-photoion coincidence techniques [31–33] culminating in using reaction microscopes (REMI) [23,34–39] that allow one for the coincident detection of the 3D vector momenta of several electrons and ions, low-energy photoelectron angular distributions from free "fixed-in-space" molecules are recorded. Here, in the present experiments, the molecular orientation is retrieved *a posteriori* via coincident detection of heavy molecular fragments making this method extremely demanding technologically and limiting it to essentially diatomic molecules where, in addition, the axial recoil approximation has to hold. Since (multi) coincidences are requested, typically less then one event per beam pulse can be accepted for a reliable analysis of the data, thus requiring MHz repetition rates from the pulsed radiation source as available at synchrotrons to take multidimensional data with sufficient statistical significance. Moreover, due to the timing properties of synchrotrons in the range of 100 ps, no short-time pump-probe experiments can be realized. Femtosecond slicing devices available at some synchrotrons do not deliver enough photons for such investigations [40]. Finally, only low-energy electrons $E_e < 50$ eV were recorded up to now (mainly due to the time-of-flight spectroscopy methods used) that make the interpretation of the data demanding. Nevertheless, scattering patterns provided detailed information to an unprecedented level about a variety of processes such as localization of charges [37] and core holes [38], interferences in molecular double-slit or multislit arrangements [39,41], phases of photoelectron waves [42,43], and last but not least, the electronic potentials and the molecular structure via photoelectron diffraction [23,44].

It also decisively extends the huge area of previous ultrafast pump-probe "femto-chemistry" studies (see Ref. [45]) performed with long-wavelength (optical) probe lasers that

can only indirectly deliver final-state (time of probe) structure information of smaller molecules based on spectroscopic knowledge of the potential curves accessed by the probe pulse. Since the potential curves along the reaction coordinate usually cannot be calculated for larger molecules, this method remained limited to smaller species.

Reaching femtosecond time scales without the need for crystallization of samples we can access a different class of molecules as well as ultrashort times, well below the picosecond time-resolved experiments recently performed at synchrotrons (see Ref. [46]).

Last but not least our method is expected to have certain advantages compared to using vuv high-harmonic radiation as a probe pulse and that has already led to the first successful measurements (see Ref. [47]). In the latter, up to now, photons are not high energetic enough at acceptable intensities to access core-level electrons and thus to specify in detail the birth location of the photoelectron. Since, in principle, attosecond time resolution can be achieved with this technology both methods might be considered as complementary.

III. THEORETICAL DESCRIPTION AND RESULTS

Let us consider the photoionization of a molecule assuming that this process can be regarded as an effectively single-electron problem. The corresponding Schrödinger equation reads

$$i\frac{\partial \Psi}{\partial t} = [\hat{H}_0 + \hat{W}_{EM}(t)]\Psi. \tag{1}$$

Here, $\Psi = \Psi(\mathbf{r}, t)$ is the electron wave function that is space and time dependent and describes the dynamics of the "active" electron in the photoionization process. Further, $\hat{H}_0$ is the Hamiltonian for the electron in the absence of the electromagnetic field and

$$\hat{W}_{\mathrm{EM}}(t) = \mathbf{A}\hat{\mathbf{p}}/c \tag{2}$$

is the interaction between the electron and the field, where $\hat{\mathbf{p}}$ is the operator for the electron momentum, $\mathbf{A}$ is the vector potential of the field, and c is the speed of light. Assuming that the field is linearly polarized we take

$$\mathbf{A}(\mathbf{r}, t) = \mathbf{A}_0 \cos(\omega_0 t - \mathbf{k}_0\mathbf{r}). \tag{3}$$

Here $\mathbf{r}$ and t are the space and time coordinates, ω_0 and $\mathbf{k}_0$ are the frequency and wave vector, and $\mathbf{A}_0 = a_0\mathbf{e}$, where $\mathbf{e}$ is the polarization vector ($\mathbf{e}\mathbf{k}_0 = 0$) and $a_0 = cF_0/\omega_0$ is the amplitude of the vector potential with F_0 being the strength of the electromagnetic field.

In the following we shall discuss two approaches to address photoionization. In one of them the process is dealt with by finding the wave function, which is a solution of Eq. (1) satisfying appropriate initial and boundary conditions and which describes the evolution of the electron wave packet in time and space. The second approach, which does not consider the space-time characteristics of the process, is based on obtaining the transition amplitude that enables one to calculate the momentum spectrum of the emitted photoelectrons. Clearly, these two approaches can be considered as complementary.

A. Approach 1

The wave function $\Psi = \Psi(\mathbf{r}, t)$ can be expanded according to

$$\Psi(t) = g(t)\psi_i(t) + \int d^3\mathbf{p}\beta_{\mathbf{p}}(t)\psi_{\mathbf{p}}^{(+)}(t), \tag{4}$$

where $\psi_i(t)$ and $\psi_{\mathbf{p}}^{(+)}(t)$ are solutions of the field-free Hamiltonian

$$i\frac{\partial \psi}{\partial t} = \hat{H}_0\psi, \tag{5}$$

for bound and continuum states of the electron, respectively, and $g(t)$ and $\beta_{\mathbf{p}}(t)$ are the time-dependent expansion coefficients.

Since, in the (tightly) bound state the electron is very well localized, we can approximate $\psi_i(t)$ as

$$\psi_i(t) = \varphi_i(\mathbf{r} - \mathbf{R}_0)\exp(-i\varepsilon_0 t), \tag{6}$$

where φ_i is the state of the electron bound in the atom, whose nucleus has the coordinates $\mathbf{R}_0$ and ε_0 is the corresponding binding energy.

To build states $\psi_{\mathbf{p}}^{(+)}(t)$ representing the stationary continuum spectrum we shall assume that the kinetic energy of the electron motion in the continuum is sufficiently high and therefore $\psi_{\mathbf{p}}^{(+)}(t)$ can be obtained in the first-order approximation in the interaction between the electron and the atomic centers constituting the molecule. This yields

$$\psi_{\mathbf{p}}^{(+)}(t) = \frac{\exp(-iE_p t)}{(2\pi)^{3/2}} \times \left\{ \exp(i\mathbf{p}\mathbf{r}) + \frac{1}{(2\pi)^{3/2}}\sum_j \exp(i\mathbf{p}\mathbf{R}_j) \times \int d^3\mathbf{p}' \frac{\widetilde{V}_j(\mathbf{p}' - \mathbf{p})}{E_p - E_{p'} + i\alpha}\exp[i\mathbf{p}'(\mathbf{r} - \mathbf{R}_j)] \right\}. \tag{7}$$

Here $\mathbf{p}$ and $E_p = p^2/2m_e$ ($p = |\mathbf{p}|$) are the momentum and energy, respectively, of the continuum state and

$$\widetilde{V}_j(\mathbf{q}) = \frac{1}{(2\pi)^{3/2}}\int d^3\mathbf{r} V_j(\mathbf{r})\exp(-i\mathbf{q}\mathbf{r}), \tag{8}$$

is the Fourier transform of the interaction $V_j(\mathbf{r}) = V_j(\mathbf{r} - \mathbf{R}_j)$ between the electron and the jth atomic center of the molecule whose nucleus is located at a point with the coordinates $\mathbf{R}_j$. In Eq. (7) $\alpha \to +0$ shows how to handle the singularity and the sum runs over all atomic centers of the molecule, $j = 0, 1, \ldots, N-1$ where N is the number of atoms, including the emitting one ($j = 0$). One should note that in Eq. (7) we neglected all inelastic channels corresponding to energy transfers between the emitted photoelectron and the internal degrees of freedom of the residual molecular ion. Note also that the state (7) is the so-called "out-state," which asymptotically (at large distances between the electron and the residual molecule) is a superposition of a plane and an outgoing scattered wave.

To obtain the unknown coefficients $g(t)$ and $\beta_{\mathbf{p}}(t)$ we insert the wave function (4) into the Schrödinger equation (1) and use the rotating-wave approximation. This leads to the following system of differential equations

$$i\frac{dg(t)}{dt} = \int d^3\mathbf{p} W_{g,\mathbf{p}} \exp(i\omega_0 t)\beta_{\mathbf{p}}(t),$$
$$i\frac{d\beta_{\mathbf{p}}(t)}{dt} = W^*_{g,\mathbf{p}} \exp(i\omega_0 t) g(t), \quad (9)$$

where

$$W_{g,\mathbf{p}} = \frac{1}{2c}\int d^3\mathbf{r}\psi_i^*(t=0)\exp(-i\mathbf{kr})(\mathbf{A}_0\hat{\mathbf{p}})\psi_{\mathbf{p}}^{(+)}(t=0). \quad (10)$$

Assuming for the moment that the electromagnetic field is suddenly switched on at $t = 0$, when the electron was in the state ψ_i, the initial conditions for the system (9) are given by $g(t=0) = 1$ and $\beta_{\mathbf{p}}(t=0) = 0$.

Here we shall not go into detail of how the system (9) can be solved and the state (4) derived and merely note that one can show that at asymptotically large distances between the photoelectron and the residual molecule the wave function $\Psi(t)$ can be presented in the following approximate form

$$\Psi(\mathbf{r},t) = \exp(-iE_e t)\left\{\frac{\exp(ip_e\xi_0)}{\xi_0}\exp[-\Gamma(t-\xi_0/v_e)]\theta(t-\xi_0/v_e)\right.$$
$$\times\sum_{l=0}^{\infty}\sum_{m=-l}^{+l} B(l_i,m_i;l,m;\boldsymbol{\xi}_0/\xi_0)$$
$$+\sum_{j\neq 0}\frac{\exp(ip_e\xi_j)}{\xi_j}\frac{\exp(ip_eR_{j0})}{R_{j0}}\exp[-\Gamma(t-(\xi_j+R_{j0})/v_e)]\theta[t-(\xi_j+R_{j0})/v_e]$$
$$\left.\times\sum_{L=0}^{\infty}\sum_{M=-L}^{+L}\sum_{l=0}^{\infty}\sum_{m=-l}^{+l} C(l_i,m_i;L,M;l,m;\boldsymbol{\xi}_j/\xi_j,\mathbf{R}_{j0}/R_{j0})\right\}. \quad (11)$$

Here, $E_e = \varepsilon_0 + \omega_0$ is the energy of the emitted electron, Γ ($\Gamma \ll E_e$) is the half-width of the initial electron state caused by the photo effect, $p_e = \sqrt{2m_eE_e}$ and $v_e = p_e/m_e$ are the absolute values of the electron momentum and velocity, respectively, $\boldsymbol{\xi}_j = \mathbf{r} - \mathbf{R}_j$, $\mathbf{R}_{j0} = \mathbf{R}_j - \mathbf{R}_0$, l_i and m_i are the angular momentum and its projection in the initial electron state ψ_i and θ is the (stepwise) θ function. The functions $B(l_i,m_i;l,m;\boldsymbol{\xi}_0/\xi_0)$ and $C(l_i,m_i;L,M;l,m;\boldsymbol{\xi}_j/\xi_j,\mathbf{R}_{j0}/R_{j0})$ have rather complicated forms and will be specified elsewhere.

The physical meaning of the state in Eq. (11) is rather transparent. This state describes an electron wave packet, which is a superposition of the wave, propagating directly from the initial electron location (the first two lines in the parentheses), and of the "secondary" waves, appearing due to the electron scattering on all other atomic centers in the molecule (the last two lines). The θ functions in Eq. (11) emphasize the fact that to traverse a distance L an electron moving with a velocity v_e needs the time L/v_e and the decaying exponential factors reflect the depletion of the electron population in the initial state due to the emission.

B. Approach 2

The spectrum of photoelectrons emitted from the molecule can be calculated using the transition amplitude

$$S_{fi} = -i\int_{-\infty}^{+\infty} dt\langle\psi_f(t)|\hat{W}_{EM}|\psi_i(t)\rangle. \quad (12)$$

where $\psi_i(t)$ is given by Eq. (6) and $\psi_f(t)$ is the so-called "in-state" for the emitted electron $\psi_f(t) = \psi_{\mathbf{p}}^{(-)}(t)$, which is obtained from the "out-state" (7) according to $\psi_{\mathbf{p}}^{(-)}(t) = [\psi_{-\mathbf{p}}^{(+)}(-t)]^*$. Inserting the states $\psi_i(t)$ and $\psi_{\mathbf{p}}^{(-)}(t)$ into Eq. (12) and integrating over the time and space coordinates we obtain

$$S_{fi} = -\frac{\pi i}{c}\exp(i\mathbf{kR}_0)G_{fi}\delta(E_p - \varepsilon_0 - \omega_0), \quad (13)$$

where

$$G_{fi} = (\mathbf{A}_0\mathbf{p})\widetilde{\varphi}_i(\mathbf{p}-\mathbf{k})\exp(-i\mathbf{pR}_0)$$
$$+\frac{1}{(2\pi)^{3/2}}\sum_j\exp(-i\mathbf{pR}_j)$$
$$\times\int d^3\mathbf{p}'\frac{\widetilde{V}_j(\mathbf{p}-\mathbf{p}')}{E_p - E_{p'} + i\alpha}$$
$$\times\exp[i\mathbf{p}'(\mathbf{R}_j-\mathbf{R}_0)](\mathbf{A}_0\mathbf{p}')\widetilde{\varphi}_i(\mathbf{p}'-\mathbf{k}). \quad (14)$$

The δ function in Eq. (13) expresses the energy conservation in the photoeffect and

$$\widetilde{\varphi}(\mathbf{q}) = \frac{1}{(2\pi)^{3/2}}\int d^3\mathbf{r}\varphi(\mathbf{r})\exp(-i\mathbf{qr}), \quad (15)$$

is the Fourier transform of the initial electron state.

Using the standard consideration for finding the momentum distribution of the photoelectrons from the transition amplitude we obtain that this distribution is given by

$$\frac{d\sigma}{d^3\mathbf{p}} = \frac{\pi}{2c^2}|G_{fi}|^2\delta(E_p - \varepsilon_0 - \omega_0). \quad (16)$$

The knowledge of the momentum distribution of the emitted electrons and the experimental geometry enables one to calculate the electron intensity on the detector.

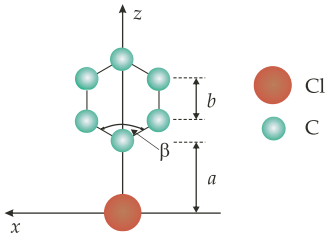

FIG. 2. (Color online) A sketch of the chlorine-benzene molecule (the H atoms are not shown): $a = 2.01$ Å, $b = 1.4$ Å, and $\beta = 2\alpha = 120^\circ$.

C. Results

In the present article we will not present results obtained with the wave function (11). Instead, assuming that $\Gamma \to 0$ and considering only the space-time points with $v_e t > \xi_j + R_{j0}$, we shall replace expression (11) by a simpler one which was earlier used in the studies of inside photoelectron holographic imaging of solids [15–17].

We take the principle scenario depicted in Fig. 1 and consider the photoionization of a chlorine-benzene molecule (see Fig. 2) from the K shell of the Cl atom by a beam of 4.5 keV FEL photons. The photons are assumed to be linearly polarized along the y axis in the case of geometry I (Fig. 3) and along the z axis in the case of geometry II (Fig. 6). The photon absorption results in the emission of a 1.7 keV electron, which scatters on the C atoms of the molecule before reaching the detector (we neglect the H atoms as scatterers because of their relatively weak field).

A monochromatic electron source p-wave Ψ_{source} is launched from the K shell of Cl by dipole transition

$$\Psi_{\text{source}} = \frac{A \exp(ip_e\xi_0)}{\xi_0} Q_1(\xi_0) Y_{1,0}(\boldsymbol{\xi}_0/\xi_0), \tag{17}$$

with the radial part Q_1 and spherical harmonic $Y_{1,0}$ describing the electron preferably ejected along the electric field vector.

In the single scattering picture, the total wave Ψ_{tot} on the detector plane is

$$\Psi_{\text{tot}} = \Psi_{\text{source}}(\boldsymbol{\xi}_0) + \sum_j f_j(\Theta_j) \frac{\exp(ip_e\xi_j)}{\xi_j} \Psi_{\text{source}}(\boldsymbol{\xi}_0 - \boldsymbol{\xi}_j). \tag{18}$$

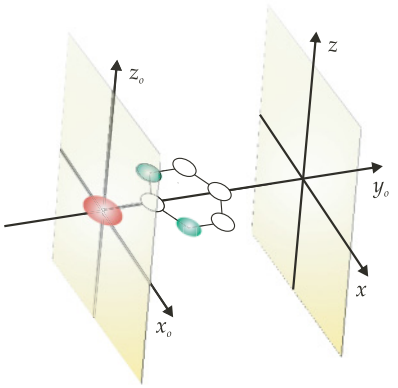

FIG. 3. (Color online) A sketch of geometry I showing the emitter (Cl atom), which is taken as the origin of the coordinate system and two "active" scatterers (C atoms) located in the x_0-y_0 plane.

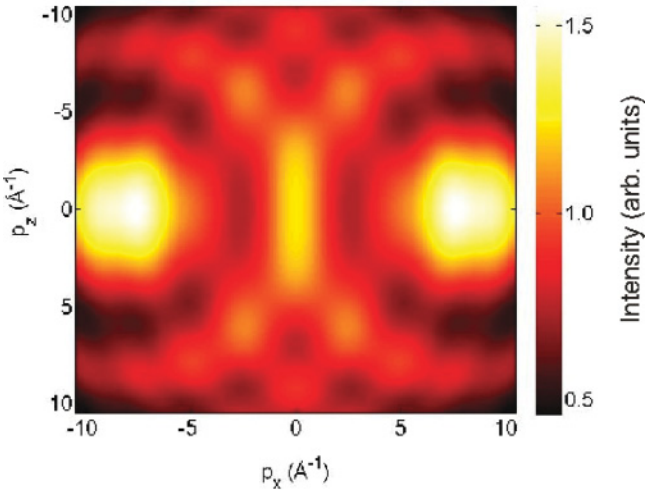

FIG. 4. (Color online) The calculated photoelectron hologram for the geometry I. Here, a 1.7 keV photoelectron emitted from the Cl atom is scattered by two C atoms.

Here Θ_j is the scattering angle and $f_j(\Theta_j)$ the scattering amplitude, which in the first Born approximation is given by

$$f_j(\Theta) = -\frac{m_e}{2\pi\hbar^2} \int d^3\xi\, V_j(\boldsymbol{\xi}) \exp(-i\mathbf{q}\boldsymbol{\xi}), \tag{19}$$

where $|\mathbf{q}| = 2p_e \sin(\Theta/2)$. The simple expression (18) should be a reasonable approximation if the size of the space, where the scattering potential V_j is effectively located, is substantially less than the distance R_{j0}. The Born approximation is safely valid for ~1 keV photoelectrons.

In a first step we take geometry I sketched in Fig. 3 and only consider two out of the six C atoms of the molecule that are marked in Fig. 3 by solid circles. The calculated hologram $I(p_x, p_z) = |\Psi_{\text{tot}}|^2$ is shown in Fig. 4. Here Ψ_{tot} is given by Eq. (18) with $p_x = ps_x$ and $p_y = ps_y$, where s_x and s_y are the components of the unit vector $\mathbf{s} = \mathbf{r}/r$ in the direction of the scattered wave, p is the magnitude of the electron momentum,

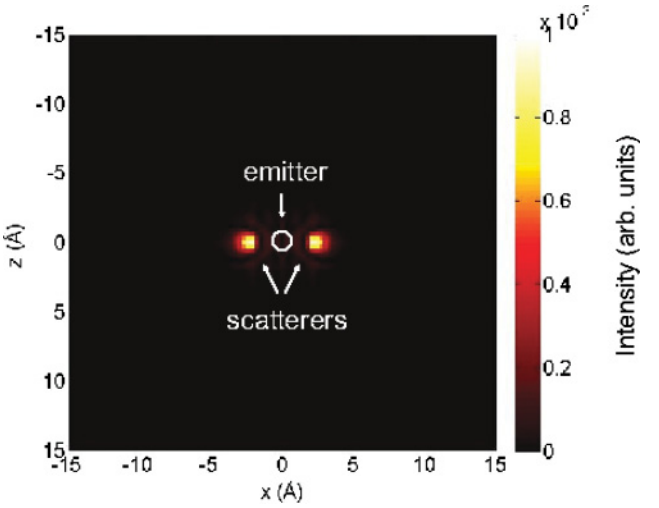

FIG. 5. (Color online) Atomic images in the plane x-z, 6 Å above the emitter, reconstructed from the hologram shown in in Fig. 4. As usual with inside-source holography, the emitter (indicated by a circle) sits at the origin of the image and is not reproduced.

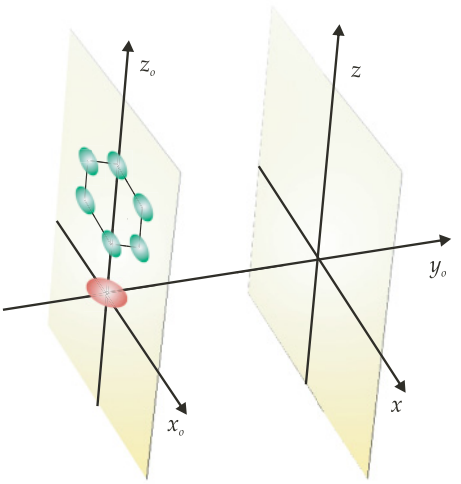

FIG. 6. (Color online) A sketch of geometry II showing the emitter (Cl atom), which is taken as the origin of the coordinate system and six scatterers (C atoms) on the x_0-z_0 plane.

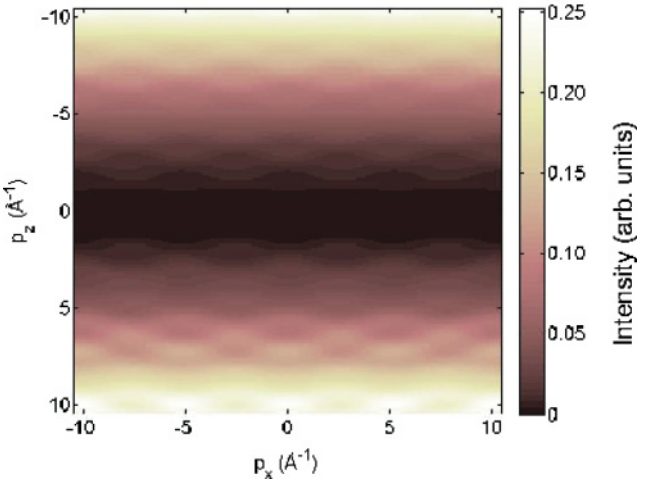

FIG. 7. (Color online) The calculated photoelectron hologram for geometry II. Here a 1.7 keV photoelectron emitted from the Cl atom is scattered by six C atoms located on the x_0-z_0 plane.

and $\mathbf{r}$ is the position vector extending from the origin of the coordinate system to the detector plane. The hologram $I(p_x, p_z)$ can be inverted by mathematical means to yield real space images that locate individual atoms surrounding the emitter (see, for instance, Fig. 5). Here we adopt a reconstruction formalism based on the Helmholtz-Kirchoff integral theorem as proposed in Ref. [22], where the amplitude of the object wave field (the atomic image function) $U(\mathbf{r})$ at any point $\mathbf{r} = x\mathbf{e}_x + y\mathbf{e}_y + z\mathbf{e}_z$ in the space near the emitter can be represented as

$$U(\mathbf{r}) \sim \int dp_x \int dp_z \chi(\mathbf{p}) \exp\left(iy\sqrt{p^2 - p_x^2 - p_z^2}\right) \times \exp(ip_x x + p_z z), \tag{20}$$

with $\chi(\mathbf{p}) = |\Psi_{\text{tot}}|^2 - |\Psi_{\text{source}}|^2$ being the oscillatory part of the hologram that contains all information about the local environment of the emitter. This expression represents the phased two-dimensional (2D) Fourier transform of $\chi(\mathbf{p})$ and can easily be calculated by applying fast Fourier transform algorithms. In principle it should be possible to achieve a sub-Ångström spatial resolution $\delta r \propto \pi/p$, however, the anisotropy of the electron scattering (with forward scattering being a major obstacle) produces artifacts in the reconstructed images that are manifested as small distortions and peak shifts from the real space images amounting to about 1 Å. Several procedures to correct these effects and thus to improve the image quality and/or extract additional information were proposed: some of them are based on the inversion formalism [17,48] whereas others exploit small changes in diffraction condition (see Ref. [29]).

Next we assume geometry II sketched in Fig. 6 and consider now all six C atoms as scatterers. In this case we obtain an interference hologram shown in Fig. 7. Retrieval of the structure yields several spots at the positions of the C nuclei as well as their mirror images (see Fig. 8).

Note also that we performed calculations for the system and geometries using the approach 2. We found that, compared to the description discussed previously, these calculations lead to holograms, which possess the same qualitative features (see for instance Fig. 9) and, thus, yield the same molecular structure.

Summarizing the previous brief discussion we can conclude that our quantum calculations that should be sufficiently accurate at this high photon energy, reveal the salient interference features due to the scattering of the outgoing photoelectron from the different atoms in the molecule and thus support the basic idea brought forward in this article.

IV. POSSIBLE TECHNICAL REALIZATION USING CHLORINE-BENZENE AS A MODEL SYSTEM

Radiation source: The Linac Coherent Light Source (LCLS) provides $N_\gamma \sim 10^{13}$ photons at up to 10 keV in 75 fs pulses at a design repetition rate of 120 Hz, which will be the basis of our estimates. We assume to focus the radiation to a spot diameter of 10 μm. Recently, lasing at 8.3 keV was demonstrated with a 10^{12} photons per pulse at a width of

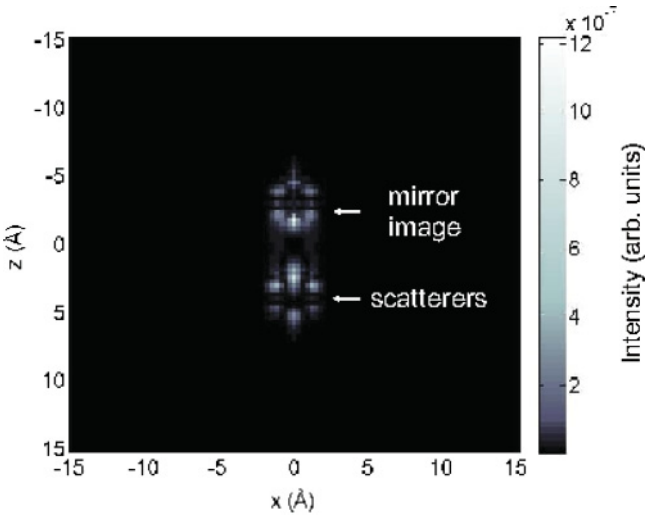

FIG. 8. (Color online) Positions of the scatterers (and the mirror image) 1 Å above the emitter retrieved from the hologram shown in Fig. 7.

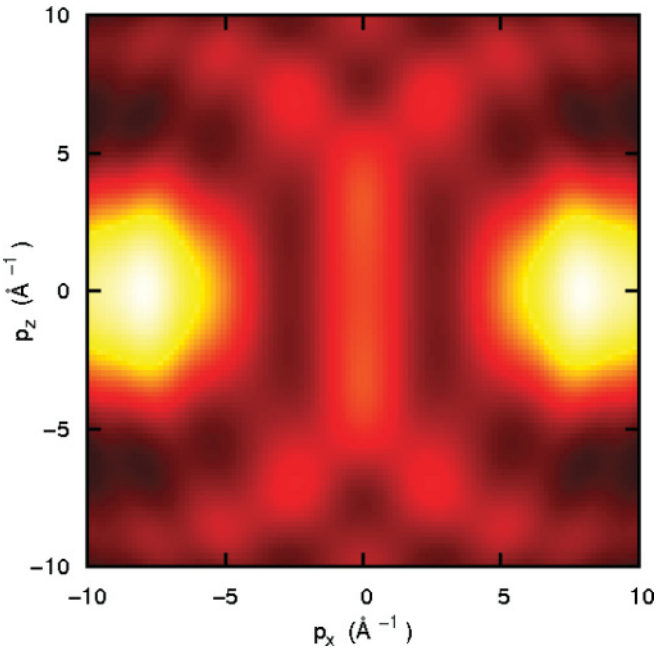

FIG. 9. (Color online) The case of geometry I. The hologram on the detector calculated using approach 2.

75 fs and beam time will be allocated in late 2010 at the x-ray pump-probe (XPP) endstation [4].

Aligned target: Rotationally cold molecules can be delivered by a supersonic jet using a pulsed Even-Lavie nozzle [49,50]. Intersecting the cold molecular jet in the interaction region with pulses from a seeded nanosecond Nd:YAG alignment laser, synchronized to the LCLS pulses yields adiabatic one-dimensional (1D) and 2D alignment of the molecular samples in space. Orientation of molecules in 1D or 2D, the latter meaning that the molecule is controlled in all three spatial dimensions, can be achieved using mixed laser and dc electric fields. Adopting the numbers put forward in one of the proposals to LCLS on coherent diffraction imaging on adiabatically aligned dibromo benzene, densities up to 10^{11} cm^{-3} 2D aligned chlorine-benzene molecules can be achieved resulting in a target line density of $\Delta x = 10^{10}$ cm^{-2} assuming a target that is 0.1 cm extended along the FEL beam direction, which will be the basis of the present estimates. Applying additional fields for orienting the molecules or even obtaining conformer-selected samples significantly decreases the target densities to values that might be as small as 10^6 cm^{-3}.

Photoelectron energies and absorption cross sections: Photon absorption can take place in any electronic state of the molecule with strongly varying cross sections. Large values are achieved close to edges, where the photon energy matches the binding energy of the respective electron resulting in typical cross sections of $\sim 10^{-18}$ cm^2 and producing low-energy photoelectrons. Above the edge, the cross section for that specific shell decreases rapidly with about $(\hbar\omega_\gamma)^{-3.5}$. Assuming that core-level electrons of the atomic constituents of the molecule are essentially characterized by their atomic energy levels and cross sections, we adopt one situation in which 4.5 keV photons irradiate the molecules. In such a case the dominant channel of the electron emission is photon absorption by the K-shell electrons of Cl with the cross section of $\sim 10^{-20}$ cm^2. The other absorption channels are not only much weaker, but also lead to the emission of electrons having much higher energies. Therefore, they can be easily separated from the main channel and in what follows will simply be ignored.

Numbers of emitted photoelectrons: Assuming an electron detection efficiency of one, we can estimate the number of recorded photoelectrons per pulse according to $N_{\rm pe} = \Delta x \sigma_{\rm photo} N_\gamma$ ending up with about $N_{\rm pe}({\rm Cl}_K) \sim 10^3$. With a repetition rate of 120 Hz the corresponding rate will be 1.2×10^5 electrons per second. To estimate the time required to record a snapshot of the molecular structure one needs, in addition, the elastic scattering cross section for the interaction of the launched photoelectrons with the atoms in the molecule on their way out, which is implicitly included in our later theoretical simulations. Taking into account the p-wave character of the emitted photoelectrons and assuming that each of them interacts with its parent molecule only, the count rate, which in addition depends on the relative orientation of the molecule with respect to the (dipolar) photoelectron emission characteristics and the position of the detector, will be between 5000 electrons/s and 60,000 electrons/s. Assuming 300,000 electrons to be detected to obtain structural information of a medium-sized molecule at a certain time delay between pump and probe pulses, a full image might be recorded in a matter of seconds to a few minutes for one time step.

From these considerations it is obvious that ultradilute samples with line densities as small as 10^6 cm^{-2} like for conformer-selected molecules only become accessible at photon energies slightly above one of the edges of the atomic constituents of the molecule exhibiting cross sections on the order of 10^{-18} cm^2 and photoelectron energies of not more than 100 eV. Nevertheless, assuming the full performance of the LCLS with repetition rates as high as 120 Hz we still end up with about 10–120 photoelectrons per second such that a measurement of the structure, again requesting about 300,000 events, will take about two to ten hours.

From these considerations it becomes also obvious that direct coherent x-ray diffraction of oriented or even conformer-selected molecules with elastic photon scattering cross sections of the order of 10^{-24} cm^2 are completely unrealistic. The same holds for FED where in the most optimistic case 10^4 electrons in 100 fs pulses might hit the target at 1 MHz repetition rate. With elastic scattering cross sections on the order of 10^{-19} cm^2 and a target line density of 10^6 molecules/cm^2 this yields a few scattered electrons per hour.

Thus, the technology presented here does indeed allow one to access a large number of samples that are of fundamental and benchmarking interest for tracing molecular dynamics during chemical reactions. For lower photoelectron energies not considered in this article, but as used presently at synchrotrons in similar time-independent experiments, the speed for taking structural images will be limited by the count rates accepted by the various detectors as well as by space charge effects blurring the image forcing one to reduce the incoming flux.

Experimental pump-probe scheme: The rearrangement dynamics of chemical reactions (e.g., molecular elimination) in oriented molecules such as, for example, chlorine-benzene and other phenyl halides (C_6H_5Br, C_6H_5I, and C_6H_5F) can be driven with femtosecond pulses heaving a photon wavelength in the range between 190 to 250 nm and focused to a spot

size which is kept more than ten times larger than the x-ray interaction region to ensure probing of a homogeneously excited area. This wavelength range is particularly important since it corresponds to the excitations of electrons of the phenyl ring and the nonbonding electron of the halogen atoms [51]. High-intensity pulses at these wavelengths (and extended up to several μm) can be generated with an optical parametric amplifier, which can be pumped by a commercial Ti:sapphire laser (e.g., 3 mJ/pulse) producing high energy near transform-limited pulses throughout the 189 nm - 20 μm range. The experimental pump-probe laser can be synchronized to the x-ray pulses of the FEL by locking it to the master laser of the electron gun; by using a dispersion-compensated and timing-stabilized fibre links, the temporal jitter between the FEL and experimental laser can be reduced down to 10 fs [52,53].

Energy Dispersive Large-Area Electron Momentum Imaging: The new method for obtaining structural information of atomic positions with Ångström resolution in molecules as a function of time via femtosecond holographic imaging of photoelectrons relies, apart from the availability of x-ray FEL's and of 2D oriented molecular samples, decisively on high-speed, large-solid-angle, energy-dispersed, quasicontinuous along two spatial dimensions, and highly efficient detection of high-energy electrons. This can be achieved, for the first time, by new solid-state pnCCD cameras, originally developed for x-ray detection at FEL's and implemented into the CFEL-ASG-Multi-Purpose (CAMP) chamber developed by the Max-Planck Advanced Study Group (ASG) at the Center for Free-Electron Laser science (CFEL) in Hamburg. The chamber along with the detectors were described in detail before [14] such that we will concentrate on the salient features and specific requirements to be fulfilled for electron detection.

Due to the pixel size of 75 μm $\times$ 75 μm over a total area of 8 cm $\times$ 8 cm we can image the electrons in a quasicontinuous way along two spatial dimensions covering a large solid angle as requested. The high granularity of the detector simultaneously ensures that large numbers of electrons, certainly 10^4 per shot, can be recoded in an energy dispersed way, which is feasible as long as each of the 10^6 pixels is hit by not more than one electron. Moreover, the unprecedentedly high frame readout rate of up to 200 Hz is adapted to the maximum FEL repetition rate at LCLS of 120 Hz, such that electrons can be recorded shot-by-shot.

More care has to be taken concerning the energy resolution of the detector, which is excellent, close to the theoretical limit (one-electron noise) for x-ray detection. Electrons, however, have to penetrate through a protecting (50 nm Al) as well a charge carrier, isolating depletion layer (40 nm SiO_2) meaning that only electrons at around 10 keV can be detected with a probability of close to 1 and reasonable energy resolution, limited by the energy loss of the electrons in the entrance layers. Thus, electrons of 500 eV to 2 keV, as considered to be ideal for the present purpose, cannot be directly monitored, but rather have to be post-accelerated toward the detector.

For that purpose, a potential grid on a voltage of 10 kV will be placed about 1 cm away from the interaction zone as depicted in Fig. 10, allowing us to accept a solid angle $\Delta\Omega/2\pi \approx 0.74$ with the pnCCD (8 cm $\times$ 8 cm) as close as 2 cm downstream of the grid. Thus, the potential grid,

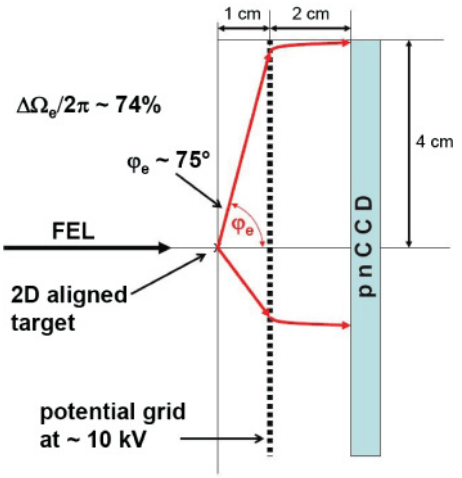

FIG. 10. (Color online) Geometry for high-energy electron detection with the pnCCD in CAMP.

serving to enhance the solid angle, at the same time post-accelerates the electrons to 10.5 or 12 keV, respectively, enabling them to penetrate into the pnCCD through various protecting and carrier depletion layers. They are then detected with a full width at half maximum (FWHM) of about 500 eV as demonstrated in a recent test measurement shown in Fig. 11 for electrons of different energies emerging from an electron microscope directly hitting (zero degree impact) the pnCCD. Thus, electrons with energies of around 1.7 or 3.5 keV emitted simultaneously in the present situation will end up with final energies of 11.7 or 13.5 keV, respectively, and thus, can be easily discriminated against each other. In practice, that means that one can, in properly chosen situations, obtain holographic images simultaneously taken at two (several) photoelectron energies, illuminating the molecule from different sites from within. On the other hand, the electron energy resolution of 500 eV clearly limits the method to cases where the photoelectrons emerging from

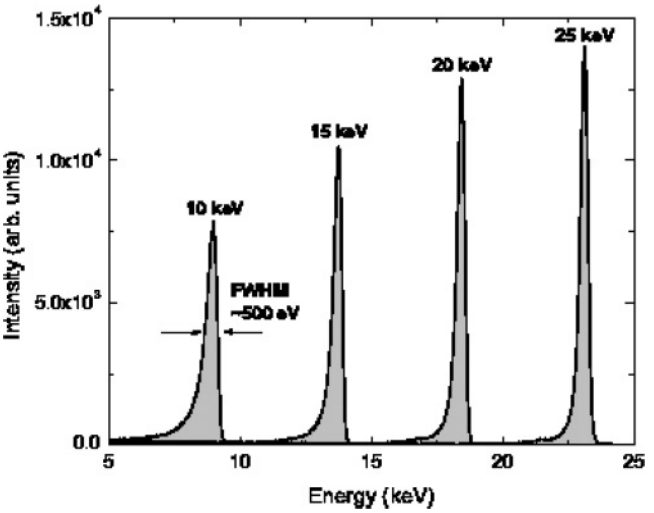

FIG. 11. Response of the pnCCD on electrons of different energies as indicated penetrating 40 nm SiO_2 insulating and 50 nm Al laser-light protection layers.

different atoms in the molecule can be cleanly separated. Ideal cases are emitters with atomic numbers between Cl ($Z = 17$) to Ga ($Z = 31$) as constituents of organic molecules containing essentially light atoms with $Z < 10$ with their K-shell energies (Cl: 2.8 keV to Ga: 10.4 keV) clearly separated from those of the lighter constituent atoms (C: 0.28 keV, H: 0.014 keV, up to F: 0.7 keV) as well as from photoelectrons emerging from the L and M shells of the heavy species. Thus, even though the situation is not completely ideal, the large selection of constituent atoms for launching electrons from within allows one to certainly choose benchmark situations for chemical dynamics. Prominent examples are all (poly) pentene rings containing one Cl atom, easily attachable at different sites as the emitter. Other molecules of interest for performing benchmarking, photoionization, or dissociation experiments might be clorethylen [54] or diphenylmethyl chloride [55].

V. SUMMARY AND OUTLOOK

We developed an idea and provided model calculations for "imaging molecules from within," which exploit the holographic diffraction pattern occurring when photoelectrons, site-specifically launched at certain atoms within molecules, are scattered off the 3D molecular potential on their way out. The observed patterns encode the 3D molecular pattern, which is retrieved with Ångström resolution using reconstruction algorithms that were developed for "inside photoelectron holography" in solid-state physics. Since femtosecond pulsed photon beams from x-ray FEL's are used to create the photoelectrons, the structure determination proceeds on an ultrafast time scale. Along with the large number of photoelectrons that are produced due the high intensity of the FEL radiation, they are perfectly suited for probing the time-dependent structure of the object under investigation in pump-probe arrangements where the dynamics are induced either by an optical pump laser or by a replica of the FEL pulse itself as recently demonstrated at the FLASH [56].

Different from any other scenario for coherent structure determination, we measure the 3D momentum vectors of high-energy electrons ($E_e > 500$ eV) with large solid angle and energy dispersed exploiting recently developed large-area pnCCD detectors along with an electric field projection technique. Along with the unique short pulse properties of the FEL, this represents the ultimate technology to obtain real-time 3D structural information for small to moderate-size molecules by providing several unique features:

(i) As the outgoing electrons are diffracted in the combined electronic and nuclear charge distribution of the molecule, the diffraction pattern does not "only" reveal information on the position of the nuclei, but moreover, on the complete multicenter molecular potential (i.e., the electronic orbitals). This is especially obvious when low-energy electrons are used to create the diffraction pattern. Thus, investigating the same reaction using photoelectrons of different energies, readily adjustable via tuning the FEL photon energies, it is expected (by comparison of the holographic images) to directly access the subtle interplay between electronic orbital and nuclear position dynamics beyond the Born-Oppenheimer approximation.

(ii) By changing the photon energy and thus the energy and the de Broglie wavelength of the emerging electron, the latter can be "adjusted" to any length scale of interest for the respective molecule, possibly even to large-scale structures such as the folding patterns of proteins, in an "inside-source holography" arrangement. Especially for larger proteins, it might, at some point, not be important to determine the position of each individual atom, but rather to monitor the motion of groups of atoms with a "fixed" structure relative to other groups.

(iii) Using high-energy photoelectron holography, it was demonstrated in solid-state physics, that the positions of up to around 50 nearest-neighbor atoms can be retrieved. Even though this seems not to be really much if the dynamics in a large molecule (e.g., a protein) shall be explored, it might be an ideal method to trace the decisive early-time dynamics around a photo receptor site.

(iv) While pump-probe experiments that study the time-dependent evolution of molecular valence orbitals were recently performed with high-harmonic laser sources [47], our approach using shorter wavelength probe pulses allows accessing localized inner-shell electrons, which is essential for structural determination via electron diffraction since it allows launching the photoelectron from specific sites within the molecule.

(v) Due to the possibility of simultaneously measuring both ions and high-energy electrons in CAMP, we will be able to continuously monitor the degree of alignment as well as the fragmentation channels (via measuring the fragment kinetic energies) in the pump-probe experiments while taking the electron diffraction data. This (quasi) coincidence mode may also allow cleaning up the experimental data in the post-analysis, especially if covariant mapping methods [57] are applied.

(vi) Since the core holes created as a consequence of photoelectron emission decay either via the emission of Auger electrons or of fluorescence photons, it should be possible (if the various energies can be separated in the pnCCD) to also record holographic images for these reaction products, as demonstrated as well in solid-state physics. Auger decays typically take place on a time scale of about 10 fs (i.e., within the present FEL pulse length) and may, in certain cases, directly influence the photoelectron emission. Radiative transitions in medium heavy atoms, on the other hand, are one to two orders of magnitude slower, and accordingly, will not affect the angular distribution of the directly emitted photo electron.

(vii) Since the intensities required for the x-ray probe pulse are rather small (large focal diameters) compared to x-ray diffraction studies (due to the fact that photoionization cross sections close to an edge are several orders of magnitude larger than x-ray scattering cross sections), radiation damage during the pulse is negligible. Furthermore, this makes photoelectron diffraction a

viable tool to study ultrathin ensembles, such as beams of conformer-selected molecules, Stark decelerated (trapped) molecules with typical target densities of only about 10^6 cm^{-3}, or ultracold (molecular) ensembles in Bose-Einstein condensates or degenerate Fermi gases. To the best of our knowledge, structural dynamics of this rather large class of samples will not be accessible by any other present technique.

ACKNOWLEDGMENTS

Support from the Max-Planck Advanced Study Group at CEFL is gratefully acknowledged. BN would like to thank DFG for support under the project VO 1278/2-1. We wish to thank Sascha Epp, Artem Rudenko, Simone Techert, Robert Moshammer, Ilme Schlichting, Robert Hartmann, Regina de Vivie-Riedle, and Henrik Stapelfeldt for helpful discussions.

[1] V. Ayvazyan *et al.*, Eur. Phys. J. **66**, 297 (2006).
[2] W. Ackermann *et al.*, Nat. Photonics **1**, 336 (2007).
[3] T. Shintake *et al.*, Nat. Photonics **2**, 555 (2008).
[4] J. Arthur *et al.*, Linca Coherent Light Source (LCLS) Conceptual Design Report No. SLAC-R.593, 2002, http://www-ssrl.slac.stanford.edu/lcls/cdr/.
[5] DESY Technical Design Report No. 2006-xxx, edited by M. Altarelli *et al.*, 2006, http://xfel.desy.de/tdr/index_eng.html.
[6] R. Neutze *et al.*, Nature (London) **406**, 752 (2000).
[7] B. Ziaja, H. Wabnitz, F. Wang, E. Weckert, and T. Moller, Phys. Rev. Lett. **102**, 205002 (2009).
[8] S. P. Hau-Riege, R. A. London, H. N. Chapman, A. Szoke, and N. Timneanu, Phys. Rev. Lett. **98**, 198302 (2007).
[9] H. Ihee *et al.*, Science **291**, 458 (2001).
[10] J. R. Dwyer *et al.*, Phyil. Trans. Soc. A **364**, 741 (2006).
[11] P. Reckenthaeler, M. Centurion, W. Fuss, S. A. Trushin, F. Krausz, and E. E. Fill, Phys. Rev. Lett. **102**, 213001 (2009).
[12] M. Meckel *et al.*, Science **320**, 1478 (2008).
[13] M. Chergui and A. H. Zewail, Chem. Phys. Chem. **10**, 28 (2009).
[14] L. Strüder *et al.*, Nucl. Instrum. Methods (to be published).
[15] J. Wider, F. Baumberger, M. Sambi, R. Gotter, A. Verdini, F. Bruno, D. Cvetko, A. Morgante, T. Greber, and J. Osterwalder, Phys. Rev. Lett. **86**, 2337 (2001).
[16] Th. Greber, J. Phys.: Condens. Matter **13**, 10561 (2001).
[17] T. Matsushita, F. Z. Guo, M. Suzuki, F. Matsui, H. Daimon, and K. Hayashi, Phys. Rev. B **78**, 144111 (2008).
[18] F. Filsinger, U. Erlekam, G. vonHelden, J. Kupper, and G. Meijer, Phys. Rev. Lett. **100**, 133003 (2008).
[19] D. Gabor, Nature (London) **161**, 777 (1948).
[20] H. D. Cohen and U. Fano, Phys. Rev. **150**, 30 (1966).
[21] M. J. Vrakking, Physics **2**, 72 (2009).
[22] J. J. Barton, Phys. Rev. Lett. **61**, 1356 (1988).
[23] A. Landers *et al.*, Phys. Rev. Lett. **87**, 013002 (2001).
[24] J. J. Larsen, K. Hald, N. Bjerre, H. Stapelfeldt, and T. Seideman, Phys. Rev. Lett. **85**, 2470 (2000).
[25] L. Holmegaard, J. H. Nielsen, I. Nevo, H. Stapelfeldt, F. Filsinger, J. Kupper, and G. Meijer, Phys. Rev. Lett. **102**, 023001 (2009).
[26] F. Filsinger *et al.*, J. Chem. Phys. **131**, 064309 (2009).
[27] H. Stapelfeldt and T. Seideman, Rev. Mod. Phys. **75**, 543 (2003).
[28] S. Y. T. van de Meerakker, H. L. Bethlem, and G. Meijer, Nature Physics **4**, 595 (2008).
[29] C. S. Fadley *et al.*, J. Phys.: Condens. Matter **13**, 10517 (2001).
[30] D. P. Woodruff, Surf. Sci. Rep. **62**, 1 (2007).
[31] A. V. Golovin *et al.*, Opt. Spectrosc. **71**, 537 (1991); Z. Phys. D **24**, 371 (1992).
[32] E. Shigemasa, J. Adachi, M. Oura, and A. Yagishita, Phys. Rev. Lett. **74**, 359 (1995).
[33] F. Heiser, O. Gessner, J. Viefhaus, K. Wieliczek, R. Hentges, and U. Becker, Phys. Rev. Lett. **79**, 2435 (1997).
[34] R. Dörner *et al.*, Phys. Rep. **330**, 95 (2000).
[35] J. Ullrich *et al.*, Rep. Prog. Phys. **66**, 1463 (2003).
[36] T. Jahnke *et al.*, Phys. Rev. Lett. **88**, 073002 (2002).
[37] F. Martin *et al.*, Science **315**, 629 (2007).
[38] M. Schoeffler *et al.*, Science **320**, 920 (2008).
[39] D. Akoury *et al.*, Science **318**, 949 (2007).
[40] R. W. Schoenlein, S. Chattopadhyay, H. H. W. Chong, T. E. Glover, P. A. Heimann, C. V. Shank, A. A. Zholents, and M. S. Zolotorev, Science **287**, 2237 (2000).
[41] D. Rolles *et al.*, Nature (London) **437**, 711 (2005).
[42] S. Motoki, J. Adachi, K. Ito, K. Ishii, K. Soejima, A. Yagishita, S. K. Semenov, and N. A. Cherepkov, Phys. Rev. Lett. **88**, 063003 (2002).
[43] O. Gessner, Y. Hikosaka, B. Zimmermann, A. Hempelmann, R. R. Lucchese, J. H. D. Eland, P. M. Guyon, and U. Becker, Phys. Rev. Lett. **88**, 193002 (2002).
[44] B. Zimmermann *et al.*, Nature Physics **4**, 649 (2008).
[45] A. H. Zewail, in *Nobel Lectures, Chemistry 1996–2000*, edited by I. Grenthe (World Scientific, Singapore, 2003).
[46] F. Schotte *et al.*, Science **300**, 1944 (2003).
[47] E. Gagnon *et al.*, Science **317**, 1374 (2007).
[48] P. M. Len, J. D. Denlinger, E. Rotenberg, S. D. Kevan, B. P. Tonner, Y. Chen, M. A. VanHove, and C. S. Fadley, Phys. Rev. B **59**, 5857 (1999).
[49] M. Hillenkamp, S. Keinan, and U. Even, J. Chem. Phys. **118**, 8699 (2003).
[50] U. Even *et al.*, J. Chem. Phys. **112**, 8068 (2000).
[51] C. Wu *et al.*, J. Chem. Phys. **121**, 8792 (2004).
[52] J. Kim *et al.*, Nature Photonics **2**, 733 (2008).
[53] J. D. Bozek, Eur. Phys. J. Special Topics **169**, 129 (2009).
[54] P. Farmanara, V. Stert, and W. Radloff, Chem. Phys. Lett. **288**, 518 (1998).
[55] B. P. Fingerhut, D. Geppert, and R. de Vivie-Riedle, Chem. Phys. **343**, 329 (2008).
[56] Y. Jiang, to be submitted (private communications).
[57] L. J. Frasinski, K. Codling, and P. A. Hatherly, Science **246**, 1029 (1989).